Available online at www.sciencedirect.com
ScienceDirect
International Journal of Thermal Sciences 46 (2007) 989–997
International Journal of Thermal Sciences
www.elsevier.com/locate/ijts

A numerical study of mixed convection in a vertical channel flow impinging on a horizontal surface

M.R.H. Nobari *, A. Beshkani

Department of Mechanical Engineering, Amirkabir University of Technology, 424 Hafez avenue PO Box 15875-4413, Tehran, Iran

Received 15 March 2006; received in revised form 24 September 2006; accepted 26 November 2006

Available online 15 February 2007

Abstract

In this study, mixed convection in a vertical channel flow discharging over a horizontal isotherm surface is investigated numerically using a finite difference method based on projection algorithm. The governing equations are discretized by a second order central difference in space and first order in time. The average Nusselt number is calculated on the horizontal surface in various vertical channels of varying areas considering non-dimensional parameters consisting of Reynolds and Richardson (or Grashof) numbers. Analysis of the results shows that there is an optimum gap to have a maximum heat transfer rate over the surface. The optimum gap value varies with Grashof and Reynolds numbers and inlet length of the channel but for high Richardson numbers, *Nu* has an increasing trend with reduction of gap size. By increasing the *Re*, *Gr* and *Ri* numbers, *Nu* number increases but in *Ri* of 0.1 and 0.01 the variations are approximately similar to each other. In addition, a divergent channel is usually more efficient than convergent one concerning heat transfer over the horizontal surface. Effects of Prandtl number and asymmetricity in channel are investigated in detail too.

Keywords: Mixed convection; Reynolds; Richardson; Finite difference; Projection method; Vertical channel

1. Introduction

Mixed convection is present where both natural and forced convection are significant in fluid flow. There are many examples for industrial applications such as cooling towers, electronic device cooling, turbine blade cooling, etc., but the configuration studied here can be used especially in flip-chips cooling problems.

The mixed convection problem is investigated by many researchers in recent decades. One of the good sources for general review of the combined convection phenomena is the book written by Gebhart et al. [1]. However, following some related published articles are cited to get more insight into the importance of the problem. Wang et al. [2] has studied mixed convection heat transfer in a horizontal open channel flow with uniform bottom heat flux, where they experimentally investigated the effect of thermal instabilities on hydrodynamic and thermal conditions. Laminar mixed convection in a partially blocked vertical channel has numerically studied by Habchi and Acharya [3]. They reported local maximum Nusselt number at the point where separated flow beyond the blockage reattaches. An experimental investigation of mixed convection from an isolated heat source module on a horizontal plate with different thicknesses has been carried out by Kang et al. [4] to study the effects of the externally induced flow on the heat transfer rate. They have found that the maximum surface temperature occurs at the top face of module in the natural convection dominated flow and at the right face of module in the forced convection dominated flow. Rahman and Carey [5] have measured mixed convection in a partial enclosure and shown that local heat transfer coefficient over the heated surface is strongly effected by the recirculation portions of flow within the enclosure as well as the impingement of the flow on the side walls. Mixed convection in an inclined channel with a discrete heat source was numerically studied by Choi and Ortega [6] to indicate the effect of the inclination angle on different convection regimes. Calmidi and Mahajan [7] have considered a numerical investigation of mixed convection over a heated horizontal surface

* Corresponding author.
E-mail address: mrnobari@aut.ac.ir (M.R.H. Nobari).

1290-0729/$ – see front matter
doi:10.1016/j.ijthermalsci.2006.11.012

Nomenclature

a, b	parameters to determine vertical channel curve
Gr	Grashof number
H	dimensionless height of the channel
h	height of the channel
k	fluid conductivity
L	dimensionless length of the channel
l	length of the channel
Nu	average Nusselt number
Nu_X	Nusselt number
P	dimensionless pressure
p	pressure
Pe	Peclet number
Pr	Prandtl number
R	dimensionless inlet length of the channel
r	inlet length of the channel
Re	Reynolds number
Re_c	corrected Reynolds number
Ri	Richardson number
T	dimensionless temperature
t	temperature
U, V	dimensionless components of velocity
u, v	x, y components of velocity
$\vec{V}$	velocity vector
X, Y	dimensionless independent variables
x, y	independent variables
W	dimensionless gap
w	gap

Greek symbols

α	thermal diffusivity
β	volume coefficient of expansion
ε	dimensionless heat source length
φ	channel wall slope
ν	cinematic viscosity
θ	dimensionless time step
ρ	density
ξ, η	independent variables for transformed space

Subscripts

L	left side of the channel
R	right side of the channel
s	surface
w	wall
in	inlet property of fluid

Superscripts

$*$	provisional velocity
n	current time
$n+1$	next time

in a partial enclosure using various pattern of flow fields. Papanicolaou and Jaluria [8–11] carried out a series of numerical studies in order to investigate the combined forced and natural convective cooling of heat-dissipating electronic components, located in a rectangular enclosure, and cooled by an external through flow of air.

Aydin [12] investigated laminar mixed convection flow of air in a square cavity. The flow in the cavity is induced by the combined shear force and buoyancy force resulting from the movement of the left wall and the differential heating of the vertical walls. Two different implementations of the thermal boundary conditions were considered in order to characterize the aiding and opposing effects of buoyancy on the forced flow. Aydin and Yang [13] studied mixed convection in a two-dimensional square enclosure with localized heating from below and symmetrical cooling from the moving side walls. They studied effect of Ri and the dimensionless heat source length (ε). They show that the effective range of the mixed convection regime becomes larger with the increasing value of heat source length. A similar problem has been investigated where the isothermal heat source at the bottom wall is replaced with a constant flux heat source [14].

Oztop and Dagtekin [15] studied steady state two-dimensional mixed convection problem in a vertical two-sided lid-driven differentially heated square cavity. The left and right moving walls have different constant temperatures while upper and bottom walls are thermally insulated. They considered three cases depending on the direction of moving walls. The heat transfer is enhanced for the case of opposing buoyancy and shear forces and for $Ri = 10$. For $Ri < 1$, the forced convection becomes dominant, the natural convection relatively weak, as a result of which Nusselt number is relatively higher. In the case of $Ri < 1$, which is the forced convection dominated regime, when the vertical walls move in is considerably enhanced regardless of which side moves upwards.

Hsu and Wang [16] presented laminar mixed convection of micropolar fluids in a square cavity with localized heat source for Newtonian and non-Newtonian fluids. They showed that, increasing the amount of Re or Gr leads to higher heat transfer coefficient, higher heat source temperature and the heat transfer coefficient is lower for a micropolar fluid, as compared to a Newtonian fluid.

In this paper, the mixed convection is studied in different vertical channels flow discharging over a horizontal flat surface. The governing equations are solved using a second order finite difference method based on Projection scheme. Due to presence of buoyancy forces, energy equation is solved in couple with momentum equations. Here, effect of various vertical channels with constant mass fluxes on heat transfer is studied in detail taking into account the governing non-dimensional parameters.

2. Governing equations

The physical domain has been shown schematically in Fig. 1. The flow impinges vertically on a horizontal flat surface and divides into two equal size branches. It should be

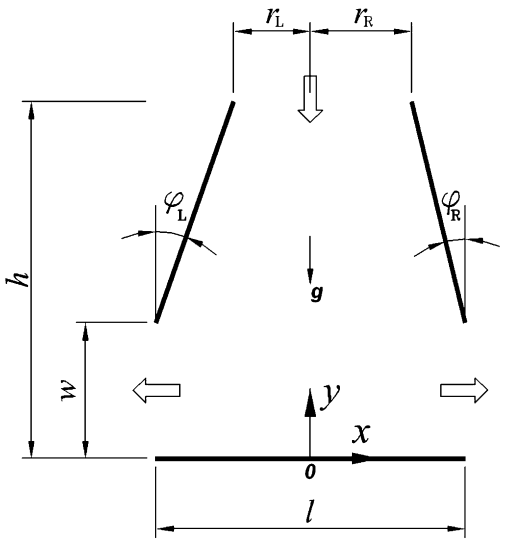

Fig. 1. Schematic of the system.

mentioned that the channel may have symmetry or asymmetry varying areas in this study.

To obtain non-dimensional governing equations, the following parameters are used

$$X=\frac{x}{l},\qquad Y=\frac{y}{l},\qquad P=\frac{p}{\rho v_{\text{in}}^2}$$

$$U=\frac{u}{v_{\text{in}}},\qquad V=\frac{v}{v_{\text{in}}},\qquad T=\frac{t-t_{\text{in}}}{t_s-t_{\text{in}}}$$

$$Re=\frac{v_{\text{in}}l}{\nu},\qquad Pr=\frac{\nu}{\alpha},\qquad Pe=Re\,Pr$$

$$Gr=\frac{g\beta(t_s-t_{\text{in}})l^3}{\nu^2},\qquad Ri=\frac{Gr}{Re^2} \tag{1}$$

Here, for thermal buoyancy effect Boussinesq approximation is used. Hence, the non-dimensional governing equations in non-conservative forms, considering two-dimensional incompressible viscous flows in presence of body forces including continuity, momentum, and energy equations are

$$\frac{\partial U}{\partial X}+\frac{\partial V}{\partial Y}=0$$

$$\left(U\frac{\partial U}{\partial X}+V\frac{\partial U}{\partial Y}\right)=-\frac{\partial P}{\partial X}+\frac{1}{Re}\left(\frac{\partial^2 U}{\partial X^2}+\frac{\partial^2 U}{\partial Y^2}\right)$$

$$\left(U\frac{\partial V}{\partial X}+V\frac{\partial V}{\partial Y}\right)=-\frac{\partial P}{\partial Y}+\frac{1}{Re}\left(\frac{\partial^2 V}{\partial X^2}+\frac{\partial^2 V}{\partial Y^2}\right)+Ri\,T$$

$$\left(U\frac{\partial T}{\partial X}+V\frac{\partial T}{\partial Y}\right)=\frac{1}{Pe}\left(\frac{\partial^2 T}{\partial X^2}+\frac{\partial^2 T}{\partial Y^2}\right) \tag{2}$$

Therefore to study the problem, the governing non-dimensional parameters including Reynolds, Richardson, and Prandtl numbers as well as non-dimensional gap and inlet length of the channel be considered. As it is clear, in mixed convection problem, all the equations are coupled and have to be solved simultaneously.

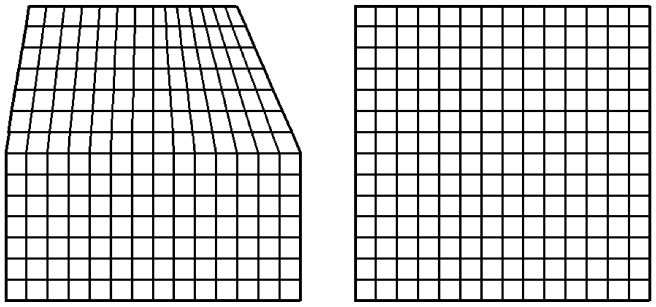

(a) (b)

Fig. 2. Physical space and the transformed computational space.

3. Grid generation

Introducing the following algebraic relations, the non-rectangular physical domain is transformed into a rectangular uniform domain which is suitable to implement the finite difference scheme (Fig. 2).

$$\begin{cases}\xi=\frac{X}{a+bY}\\ \eta=Y\end{cases}$$

$$a,b=\begin{cases}1.0,0.0 & Y<W\\ 1.0+2W\tan(\varphi_L),-2\tan(\varphi_L) & Y\geqslant W,X<0\\ 1.0+2W\tan(\varphi_R),-2\tan(\varphi_R) & Y\geqslant W,X\geqslant 0\end{cases} \tag{3}$$

where non-dimensional gap (W) and non-dimensional inlet length of the channel (R) are defined as follows (for a symmetric channel, left and right inlet lengths are equal)

$$W=\frac{w}{l},\qquad R=R_L+R_R=\frac{r_L}{l}+\frac{r_R}{l} \tag{4}$$

In this way, the governing equations are transformed from physical space to computational space considering the computed Jacobean, as follow [17]

$$J=\frac{1.0}{a+bY} \tag{5}$$

and hence the partial derivatives convert to the following forms

$$\frac{\partial f}{\partial X}=J\frac{\partial f}{\partial \xi},\qquad \frac{\partial f}{\partial Y}=\frac{\partial f}{\partial \eta}-b\xi J\frac{\partial f}{\partial \xi}$$

$$\nabla^2 f=J^2\left(1+b^2\xi^2\right)\frac{\partial^2 f}{\partial \xi^2}-2b\xi J\frac{\partial^2 f}{\partial \xi\,\eta}+2b^2J^2\xi\frac{\partial f}{\partial \xi}+\frac{\partial^2 f}{\partial \eta^2} \tag{6}$$

where, f is a general function and could be U, V, P and T.

Therefore, the transformed non-dimensional governing equations in computational domain are

$$J\frac{\partial U}{\partial \xi}+\frac{\partial V}{\partial \eta}-b\xi J\frac{\partial V}{\partial \xi}=0$$

$$\left(UJ\frac{\partial U}{\partial \xi}+V\frac{\partial U}{\partial \eta}-Vb\xi J\frac{\partial U}{\partial \xi}\right)=-J\frac{\partial P}{\partial \xi}+\frac{1}{Re}\left(J^2\left(1+b^2\xi^2\right)\frac{\partial^2 U}{\partial \xi^2}-2b\xi J\frac{\partial^2 U}{\partial \xi\,\eta}\right.$$

$$+2b^2J^2\xi\frac{\partial U}{\partial\xi}+\frac{\partial^2U}{\partial\eta^2}\Bigg)$$

$$\left(UJ\frac{\partial V}{\partial\xi}+V\frac{\partial V}{\partial\eta}-Vb\xi J\frac{\partial V}{\partial\xi}\right)$$

$$=-\frac{\partial P}{\partial\eta}+b\xi J\frac{\partial P}{\partial\xi}+\frac{1}{Re}\Bigg(J^2\left(1+b^2\xi^2\right)\frac{\partial^2V}{\partial\xi^2}-2b\xi J\frac{\partial^2V}{\partial\xi\eta}$$

$$+2b^2J^2\xi\frac{\partial V}{\partial\xi}+\frac{\partial^2U}{\partial\eta^2}\Bigg)+RiT$$

$$\left(UJ\frac{\partial T}{\partial\xi}+V\frac{\partial T}{\partial\eta}-Vb\xi J\frac{\partial T}{\partial\xi}\right)$$

$$=\frac{1}{Pe}\Bigg(J^2\left(1+b^2\xi^2\right)\frac{\partial^2T}{\partial\xi^2}-2b\xi J\frac{\partial^2T}{\partial\xi\eta}$$

$$+2b^2J^2\xi\frac{\partial T}{\partial\xi}+\frac{\partial^2T}{\partial\eta^2}\Bigg) \tag{7}$$

4. Numerical solving method

To solve the governing equations, a staggered mesh is used to discretize the equations and the following boundary conditions are implemented

(1) On the channel walls, no-slip and adiabatic conditions are employed.
(2) On the horizontal flat surface, no-slip and isothermal conditions are used.
(3) In the inlet, uniform velocity and temperature are considered.
(4) In the outlet, fully developed conditions are assumed for temperature and velocity.

Projection algorithm is used to solve the governing equations. This explicit method is a fractional step method with first order accuracy in time [18]. At the first step, provisional velocity is computed with

$$\frac{\vec{V}^*-\vec{V}^n}{\Delta\theta}+\left(\left(\vec{V}.\nabla\right)\vec{V}\right)^n=\frac{1}{Re}\left(\nabla^2\vec{V}\right)^n \tag{8}$$

This is the momentum equation without a pressure gradient. Then, at the second step, provisional velocity is corrected by considering the following equations

$$\frac{\vec{V}^{n+1}-\vec{V}^*}{\Delta\theta}+\nabla P^{n+1}=0 \tag{9}$$

The continuity is

$$\nabla.\vec{V}^{n+1}=0 \tag{10}$$

Taking the divergence of Eq. (9) and use of Eq. (10), the Poisson equation for the pressure field results as

$$\nabla^2P^{n+1}=\frac{1}{\Delta\theta}\nabla.\vec{V}^* \tag{11}$$

In this method, Neumann boundary conditions are used for pressure at all boundaries

$$\left.\frac{\partial P}{\partial\vec{n}}\right|_{\text{Boundary}}=0.0 \tag{12}$$

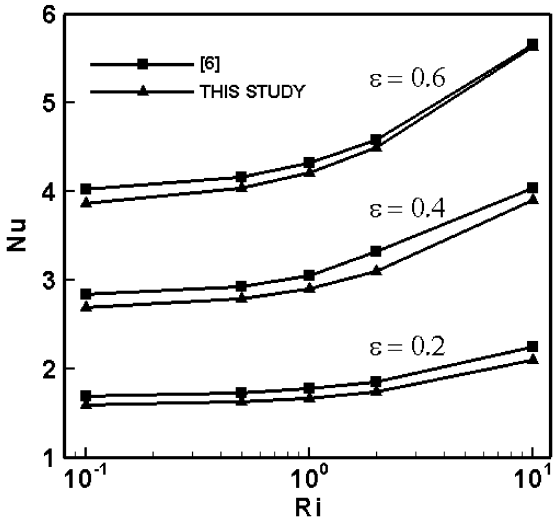

Fig. 3. Nusselt number along the isothermal heat source of the bottom wall for this study and [6].

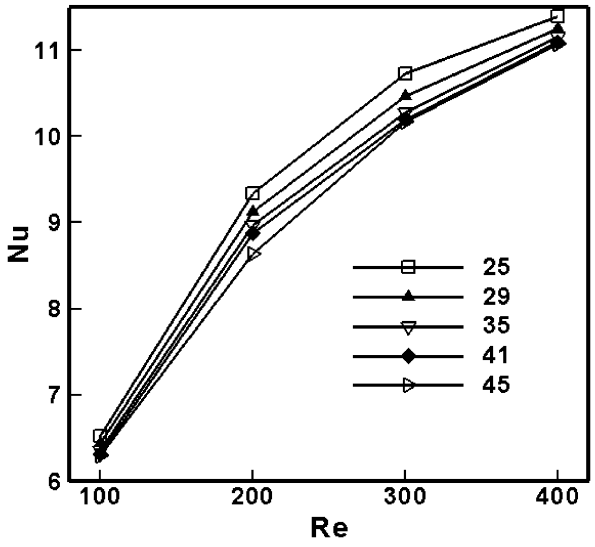

Fig. 4. Grid independency of numerical simulation test for $Pr = 0.7$, $W = 0.5$, $Gr = 2500$, $R = 0.4$.

Due to the lack of experimental data on the particular problem along with its associated boundary conditions investigated in this study, validation of the predictions could not be done against experiment. However, the case of Aydin and Yang [13] with symmetric isothermal heat source at the bottom wall was reproduced. A comparison of the variation of the Nusselt number along the isothermal heat source of the bottom wall, predicted by Aydin and this study is shown in Fig. 3 where the agreement is found to be good, and the small deviation stems from the difference in resolution.

To test grid independency of the numerical simulation, the problem has been solved in different mesh sizes. For this reason, the governing equations have been solved for 25×25, 29×29, 35×35, 41×41 and 45×45 mesh sizes. Fig. 4 shows *Nu* versus *Re* in various mesh sizes in $Pr = 0.7$, $Gr = 25000$, $W = 0.5$ and $R = 0.4$. The figure shows the solution is inde-

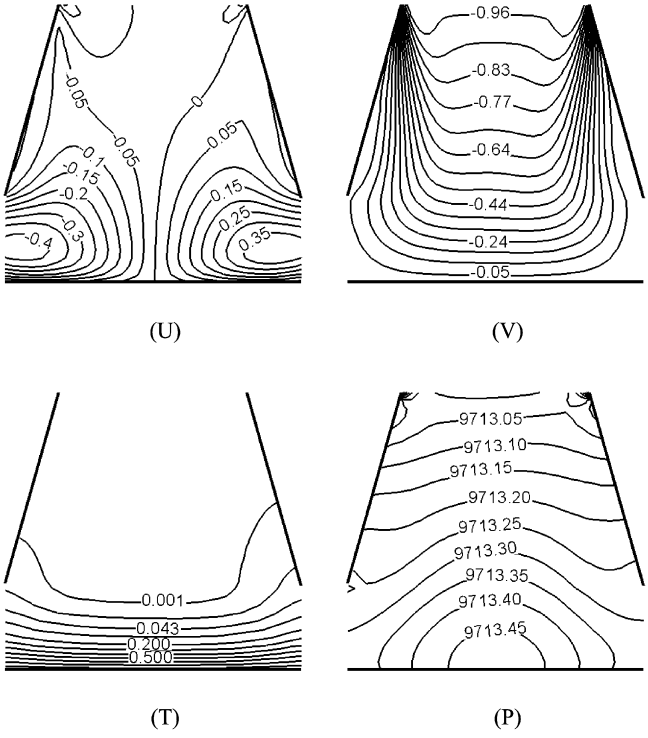

Fig. 5. Velocity, temperature and pressure contours for $\varphi = 15°$, $Re = 150$, $Ri = 0.1$, $Pr = 0.7$, $W = 0.3$.

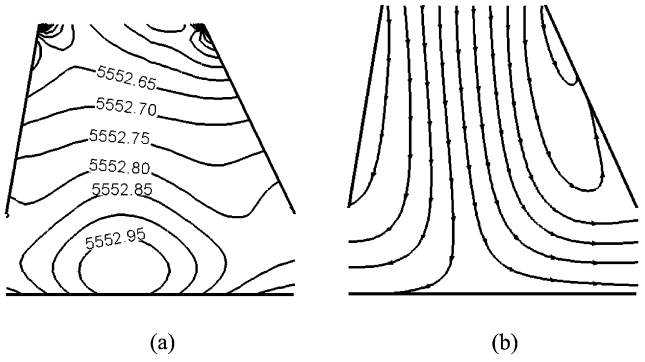

Fig. 6. Pressure contours and streamlines for $Re = 100$, $Ri = 1.0$, $\varphi_L = 10°$ and $\varphi_R = 25°$, $Pr = 0.7$, $W = 0.3$.

pendent of the grid, for convenience a grid of 35 × 35 is used for the rest cases.

5. Results and discussion

The numerical results obtained here investigate the effects of geometrical non-dimensional parameters including exit gaps (W) and channel inlet length (R), and physical dimensionless parameters consisting of Reynolds, Richardson, Grashof, Prandtl, and Nusselt numbers on the heat transfer over the horizontal surface admitting the vertical channel flow. Furthermore, the optimum gap size to have a maximum heat transfer rate on the horizontal surface is studied in detail. This point along with the generality of vertical channel geometry distinguish present article from other similar researches.

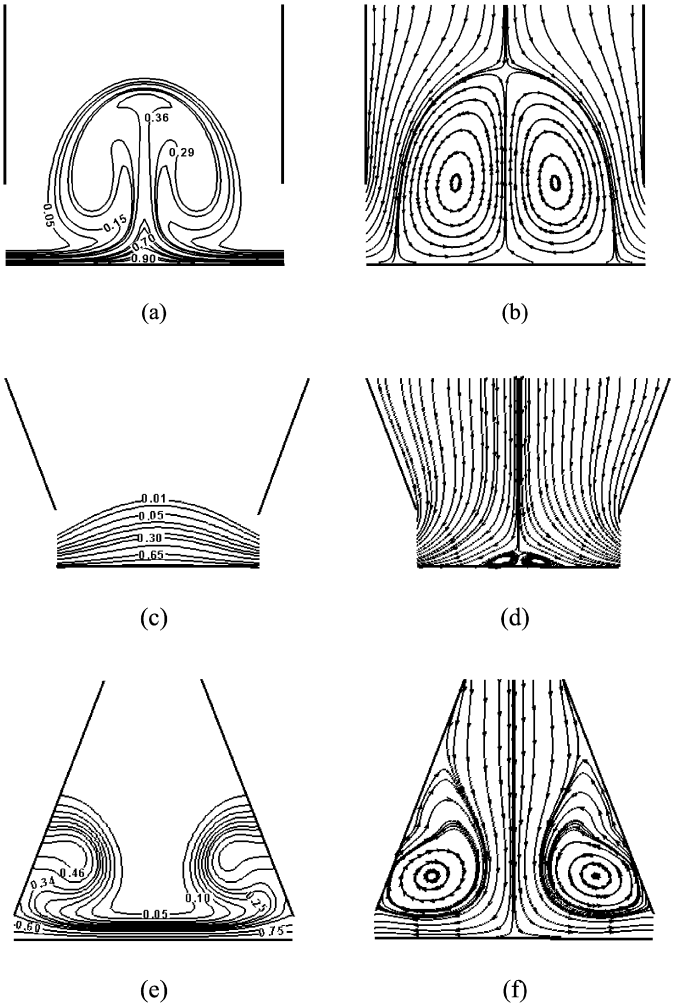

Fig. 7. Temperature contours and streamlines for $\varphi = 0°$, $Pr = 0.7$, $Re = 225$, $Ri = 10.0$, $W = 0.3$ (a), (b), $\varphi = -20°$, $Re = 150$, $Ri = 1.0$, $W = 0.3$ (c), (d), $\varphi = 8°$, $Re = 100$, $Ri = 10.0$, $W = 0.1$ (e), (f).

As already mentioned, for all the cases to be discussed here, the mesh is considered uniform with 35 by 35 divisions in x and y directions. In addition, unless otherwise specified, $\varphi_L = \varphi_R = \varphi$ ($r_R = r_L = r/2.0$), Pr is 0.7 and W is 0.3. Height and length of the channel are assumed to be equal ($l = h$), and the average Nusselt number (Nu) is computed from integrating the non-dimensional temperature gradient on the surface

$$Nu = \int Nu_X \, dX \rightarrow Nu = \int_{-0.5}^{0.5} -\left[\frac{\partial T}{\partial Y}\right]_{Y=0} dX \tag{13}$$

The governing equations are solved for Re between 50 and 500, Pr from 0.7 to 5, Gr from 10^3 to 5×10^5, inlet length of the channel from 0.25 to 1.4, and dimensionless gap from 0.1 to 0.5 in different cases.

Fig. 5 shows velocity, temperature and pressure contours for $\varphi = 15°$, $Re = 150$ and $Ri = 0.1$, where forced convection is dominant and large variations appear in the pressure, temperature, and velocity fields on the horizontal surface around stagnation point.

Fig. 6 shows effect of asymmetry of the vertical channel on pressure contours and streamlines for $Re = 100$, $Ri = 1.0$, $\varphi_L = 10^\circ$ and $\varphi_R = 25^\circ$. The contours become asymmetric and the stagnation point move toward left side that has more inlet length than the other side.

To investigate buoyancy induced flow over the horizontal surface, the Richardson numbers of 1 and 10 are taken into account. Fig. 7 shows temperature contours and streamlines for $\varphi = 0^\circ$, $Re = 225$, $Ri = 10.0$ (a), (b), $\varphi = -20^\circ$, $Re = 150$, $Ri = 1.0$ (c), (d), and $\varphi = 20^\circ$, $Re = 100$, $Ri = 10.0$, $W = 0.1$ (e), (f). As it is clear, for the case $Ri = 10$, buoyancy effects are large resulting in strong vortices with major variations in temperature field on the horizontal surface. The depth of variations of physical parameters is as high as the horizontal surface length. Several runs at different Richardson numbers indicate that for $Ri > 4$ a pair of vortices start forming on the horizontal surface accompanied by significant changes in the flow pattern and temperature field. In Fig. 8, the exit velocity profiles for the three cases represented in Fig. 7 are shown to make clear a very good satisfaction of conservation of mass.

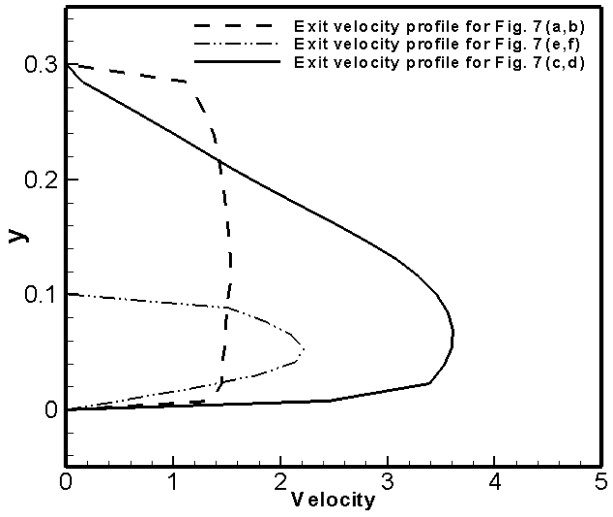

Fig. 8. Exit velocity profile for the three cases of Fig. 7.

Fig. 9 shows streamlines and dimensionless temperature gradient on the surface, for $\varphi = 15^\circ$, $Ri = 0.01$ and $Re = 100$. From the figure, it can be realized that a maximum temperature gradient occurs at the stagnation point where the flow breaks into two branches ($X = 0$).

Since the main objective of the problem studied here is to find out the case with maximum heat transfer rate and the optimum gap size concerning this. Therefore, the rest results concentrate on the average Nusselt number variation with other governing parameters. Fig. 10 shows Nu versus Re for various Gr's where $R = 0.5$. Increasing Re and Gr increases Nu indicating augmentation of heat transfer rate. In addition, for high Re ($Re > 200$) and $10^3 < Gr < 10^5$ the increase rate of heat transfer is approximately the same due to reduction of buoyancy flow driven effects and when velocity becomes 1.5 times (Re varies from 200 to 300), Nu increases by 30% for $10^3 < Gr < 10^5$.

In order to compare channels with different W (0.1, 0.2, 0.3, 0.4, and 0.5) and R, the mass flow rate of the channel is held constant. The defined Reynolds number is proportional to the mass flow rate at $\varphi = 0^\circ$, to set mass flow rate equal, a corrected Reynolds is defined as

$$Re_C = \frac{Re}{R} \tag{14}$$

Figs. 11(a)–(d) show Nu versus various values of W and R for different numbers of Re and Gr, where mass flow rate is constant for all cases. The numerical results indicate that, there is an optimum gap at which a maximum heat transfer rate over the horizontal surface occurs. For Re =50 and $Gr = 2500$ (Fig. 11(a)), the value of optimum gap varies between 0.3 and 0.4 depending on the channel inlet length (R). As R decreases both Nu and optimum gap size increases, indicating that a divergent vertical channel is more suitable to have larger heat transfer rate than a convergent channel, and the more divergent the channel is, the higher the heat transfer rate is. The physical reason to this stems from the fact that in divergent channels recirculation flow generated from separation strengthen the buoyancy driven effects which augments heat transfer rate. Cor-

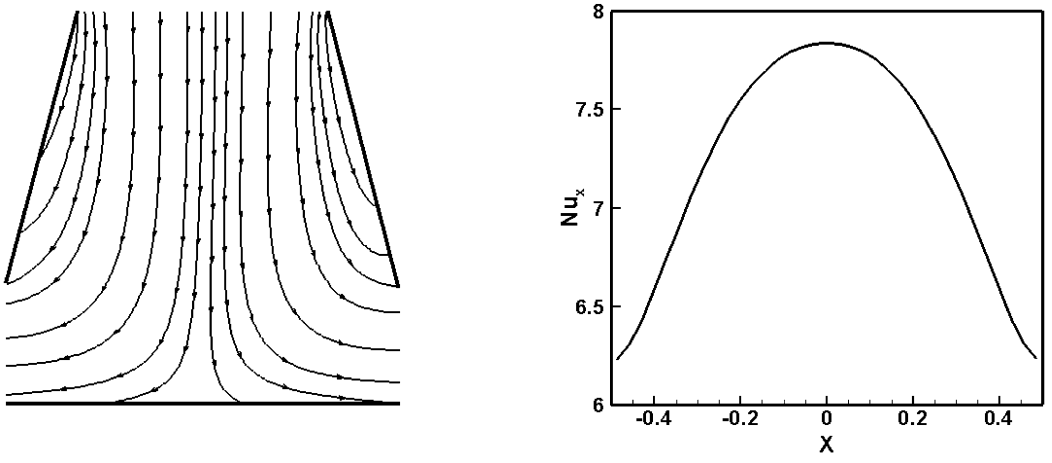

Fig. 9. Stream lines (a) and temperature gradient (b), for $\varphi = 15^\circ$, $Ri = 0.01$, $Re = 100$, $Pr = 0.7$, $W = 0.3$.

respondingly, the optimum gap size for $Re = 100$ and $Gr = 10^4$ (Fig. 11(b)) takes place at 0.25 for different values of R. This case is related to $Ri = 1$, where both forced and natural convection effects present at the same weight. In Figs. 11(c) and 11(d) where buoyancy driven flow is dominant, the optimum gap size for maximum heat transfer only exists at values of $R \leqslant 0.35$, and at $R > 0.35$, the less the gap size is, the maximum the heat transfer rate is.

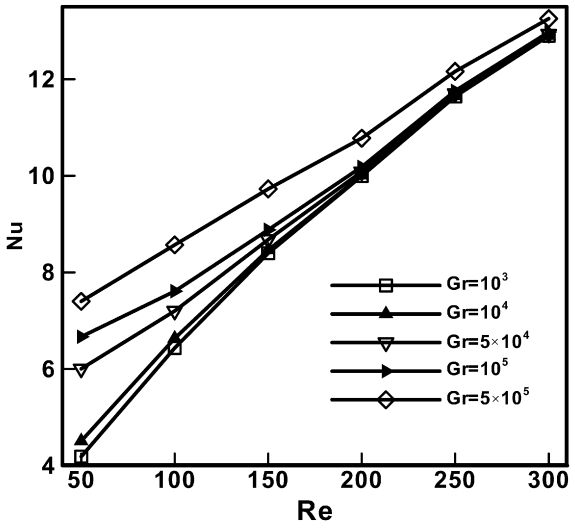

Fig. 10. *Nu* versus *Re* in various *Gr* for $R = 0.5$, $Pr = 0.7$, $W = 0.3$.

Fig. 12 shows *Nu* versus *W* in various *Re* at $Gr = 5 \times 10^3$ and $R = 0.5$ for case (a), and $Gr = 5 \times 10^4$ and $R = 0.7$ for case (b). In Fig. 12(a), W_{opt} is between about 0.2 and 0.35 for $100 < Re < 400$, but in Fig 12(b), where *Gr* is higher than (a), *Nu* has an increasing trend with *W* reduction independent of gap value.

In Figs. 13(a)–(b), *Nu* versus *W* in various *Ri* are shown at $R = 0.5$ and $Re = 100$ (a) and $R = 0.75$ and $Re = 66.66$ (b) (the mass flow rate hold constant for two cases), where for low Richardson numbers ($0.01 < Ri < 1.0$), $W_{opt} = 0.35$ and $W_{opt} = 0.25$ respectively, but *Nu* has an increasing trend with *W* reduction in higher *Ri*.

Although the curves have the same trend for *Ri* from 0.01 to 1, the heat transfer rate for the case b is about 15 percent higher than that of case a. To investigate the asymmetry effect in channel, Fig. 14 shows *Nu* versus *W* at $Re = 100$ and $Gr = 10^4$

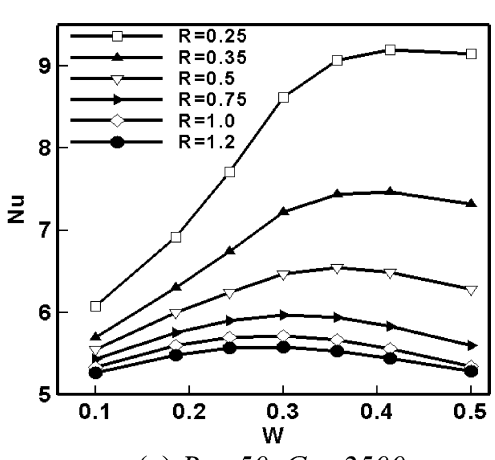

(a) *Re=50, Gr=2500*

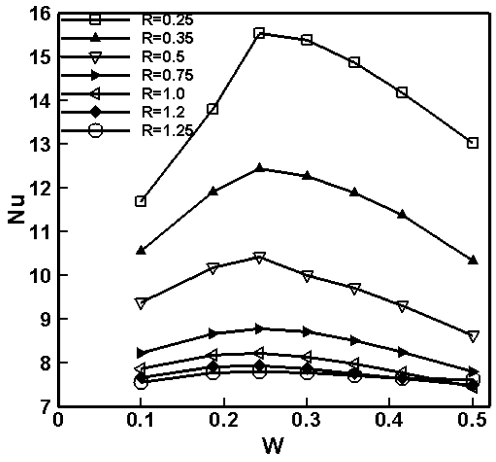

(b) *Re=100, Gr=10^4*

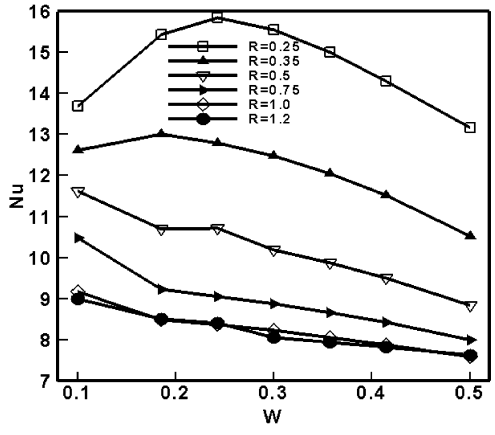

(c) *Re=100, Gr=10^5*

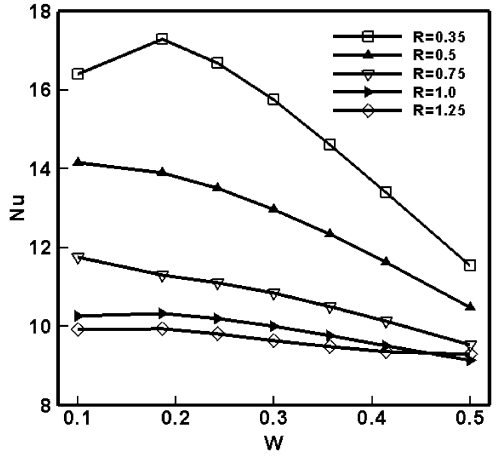

(d) *Re=150, Gr=10^5*

Fig. 11. Effect of *Re* and *Gr* on *Nu* in various *W* and *R* in constant mass flow rate at $Pr = 0.7$.

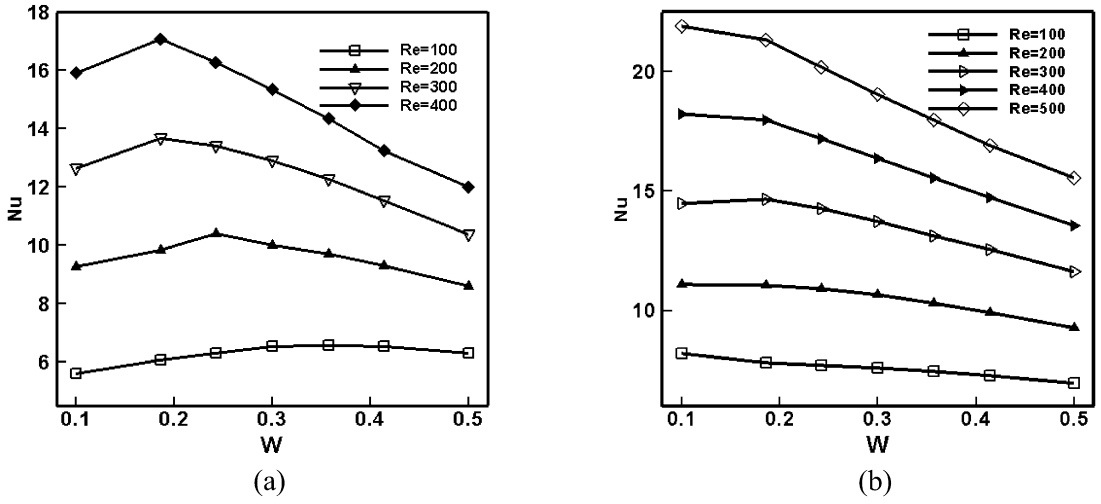

Fig. 12. *Nu* versus W in various *Re* for $Pr = 0.7$, $Gr = 5 \times 10^3$, $R = 0.5$ (a) and $Gr = 5 \times 10^4$, $R = 0.7$ (b).

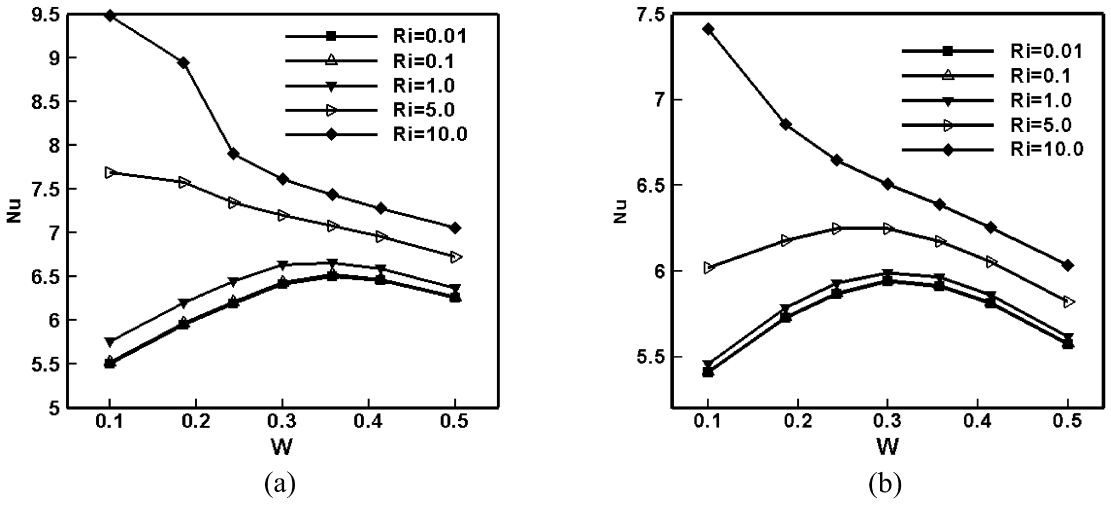

Fig. 13. *Nu* versus W in various *Ri* for $R = 0.5$, $Pr = 0.7$, $Re = 100$ (a) and $R = 0.75$, $Re = 66.66$ (b).

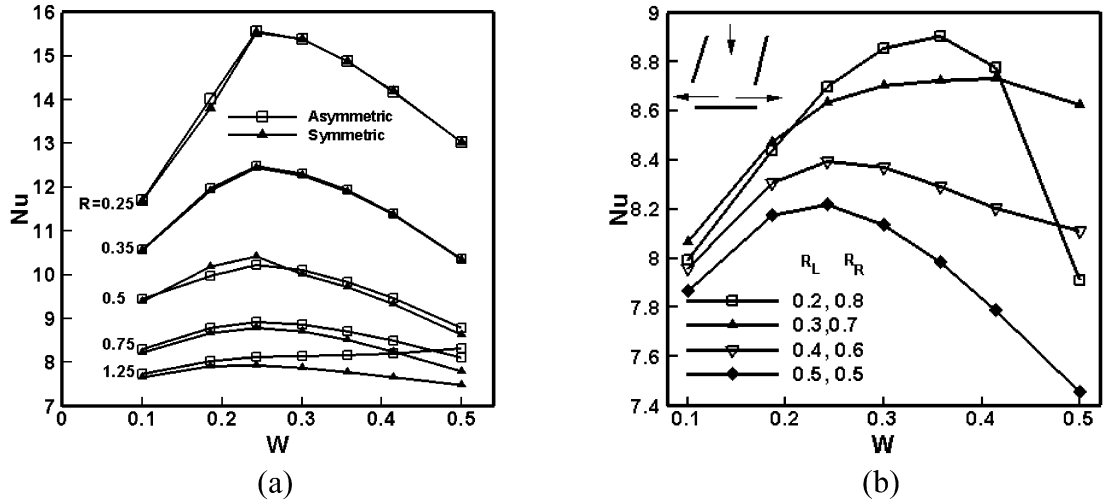

Fig. 14. Effect of asymmetricity in channel on *Nu* for $R_L = 0.6R$, $Pr = 0.7$, $Re = 100$ and $Gr = 10^4$.

for different values of R_L and R_R. Considering Fig. 14(a), for low asymmetry in channel and $R = R_L + R_R = \text{constant}$, *Nu* keep constant but for convergent channel and high gap value, asymmetric channel is more efficient than symmetric channel. In Fig. 14(b) the value of inlet length is held constant ($R = 1.0$) to investigate effect of asymmetricity amount in channel on so-

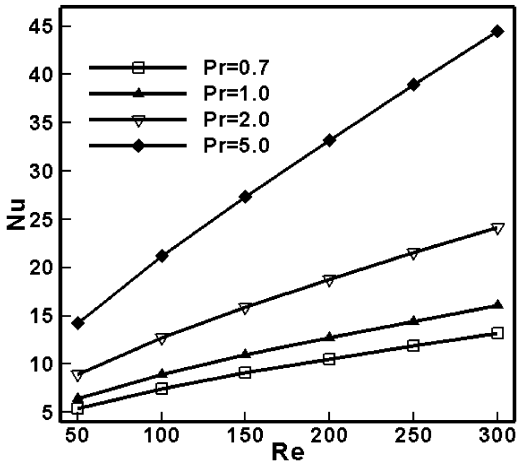

Fig. 15. *Nu* versus *Re* in various *Pr* for $R = 1.0$, $W = 0.5$, $Pr = 0.7$, $Gr = 10^4$.

lution. The figure indicates that, when the channel becomes more asymmetric ($R_L = 0.2$), *Nu* increases proportional to symmetric channel ($R_L = 0.5$).

Fig. 15 shows *Nu* versus *Re* in various *Pr* of 0.7, 1.0, 2.0 and 5.0 for $R = 1.0$, $W = 0.5$ and $Gr = 10^4$. Increasing *Pr* increases *Nu* linearly and despite the factor of 7 increases in the *Pr* number from air (0.7) to water (5), the *Nu* number varies by 200 percents in high *Re*.

6. Summary and conclusion

Mixed convection heat transfer in a vertical channel flow impinging over horizontal surface is studied taking into account a general geometry including symmetric and asymmetric divergent or convergent channels. The numerical simulation based on a second order finite difference method using projection scheme are carried out to solve governing equations. The numerical results obtained indicate the following physical points

(1) Heat transfer rate over the horizontal surface for divergent channel due to buoyancy driven flow is greater than convergent ones.
(2) In divergent channels, by increasing vertical channel inlet length, the heat transfer rate increases due to augmented buoyancy effects.
(3) Heat transfer rate for asymmetric channels are greater than symmetric channels, and the more asymmetric channel is, the greater heat transfer rate is.
(4) There is an optimum gap to have a maximum heat transfer rate over the horizontal surface for $Ri \leqslant 1$. This value varies from 0.20 to 0.35 depending on *Re*, *Gr* and *R*. For high Richardson numbers ($Ri > 1$), *Nu* has an increasing trend with reduction of gap size.

References

[1] B. Gebhart, Y. Jaluria, R.L. Mahajan, B. Sammakia, Buoyancy Induced Flow and Transport, Hemisphere, Washington, DC, 1988.
[2] G.S. Wang, F.P. Incropera, R. Viskanta, Mixed convection heat transfer in a horizontal open-channel flow with uniform bottom heat flux, J. Heat Transfer 105 (1983) 817–822.
[3] S. Habchi, S. Acharya, Laminar mixed convection in a partially blocked vertical channel, Int. J. Heat Mass Transfer 29 (1986) 1711–1722.
[4] B.H. Kang, Y. Jaluria, S.S. Tewari, Mixed convection transport from an isolated heat source module on a horizontal plate, J. Heat Transfer 112 (1990) 653–661.
[5] M.M. Rahman, V.P. Carey, Experimental measurements of orthogonal mixed convection in a partial enclosure, Int. J. Heat Mass Transfer 33 (1990) 1307–1319.
[6] C.Y. Choi, A. Ortega, Mixed convection in an inclined channel with a discrete heat source, Int. J. Heat Mass Transfer 36 (1993) 3119–3134.
[7] V.V. Calmidi, R.L. Mahajan, Mixed convection over a heated horizontal surface in a partial enclosure, Int. J. Heat Fluid Flow 19 (1998) 358–367.
[8] E. Papanicolaou, Y. Jaluria, Mixed convection from an isolated heat source in a rectangular enclosure, Numer. Heat Transfer, Part A 18 (1990) 427–461.
[9] E. Papanicolaou, Y. Jaluria, Transition to a periodic regime in mixed convection in a square cavity, J. Fluid Mech. 239 (1992) 489–509.
[10] E. Papanicolaou, Y. Jaluria, Mixed convection from a localized heat source in a cavity with conducting walls: A numerical study, Numer. Heat Transfer, Part A 23 (1993) 463–484.
[11] E. Papanicolaou, Y. Jaluria, Mixed convection from simulated electronic components at varying relative positions in a cavity, J. Heat Transfer 116 (1994) 960–970.
[12] O. Aydin, Aiding and opposing mechanisms of mixed convection in a shear and buoyancy driven cavity, Int. Commun. Heat Mass Transfer 26 (1999) 1019–1028.
[13] O. Aydin, W.J. Yang, Mixed convection in cavities with a locally heated lower wall and moving sidewalls, Numer. Heat Transfer, Part A 37 (2000) 695–710.
[14] G. Guo, M.A.R. Sharif, Mixed convection in rectangular cavities at various aspect ratios with moving isothermal sidewalls and constant flux heat source on the bottom wall, Int. J. Thermal Sci. 43 (2004) 465–475.
[15] H.F. Oztop, I. Dagtekin, Mixed convection in two-sided lid-driven differentially heated square cavity, Int. J. Heat Mass Transfer 47 (2004) 1761–1769.
[16] T.H. Hsu, S.G. Wang, Mixed convection of micropolar fluids in a cavity, Int. J. Heat Mass Transfer 43 (2000) 1563–1572.
[17] K.A. Hoffmann, S.T. Chiang, Computational Fluid Dynamics for Engineers, vol. I, Pineridge Press, 1993.
[18] R.W. Johnson, The Handbook of Fluid Dynamics, Springer, Berlin, 1998.